HELDA
HELSINGIN YLIOPISTO
HELSINGFORS UNIVERSITET
UNIVERSITY OF HELSINKI

UNIVERSITY OF HELSINKI

https://helda.helsinki.fi

Surface energy budget at Curiosity through observations and column modeling

Savijärvi, Hannu

2022-04

Savijärvi , H , Martinez , G M , Vicente-Retortillo , A & Harri , A-M 2022 , ' Surface energy budget at Curiosity through observations and column modeling ' , Icarus , vol. 376 , 114900 . https://doi.org/10.1016/j

http://hdl.handle.net/10138/344226
https://doi.org/10.1016/j.icarus.2022.114900

cc_by
publishedVersion

Downloaded from Helda, University of Helsinki institutional repository.

This is an electronic reprint of the original article.

This reprint may differ from the original in pagination and typographic detail.

Please cite the original version.

Icarus 376 (2022) 114900

Contents lists available at ScienceDirect

Icarus

journal homepage: www.elsevier.com/locate/icarus

Surface energy budget at Curiosity through observations and column modeling

H.I. Savijärvi [a,b,*], G.M. Martinez [c,d], A. Vicente-Retortillo [e,c], A.-M. Harri [b]

[a] Institute for Atmospheric and Earth System Research/Physics, University of Helsinki, Finland
[b] Finnish Meteorological Institute, Helsinki, Finland
[c] Department of Climate and Space Sciences and Engineering, University of Michigan, Ann Arbor, MI, USA
[d] Lunar and Planetary Institute, Universities Space Research Association, Houston, TX, USA
[e] Centro de Astrobiologia (INTA-CSIC), Madrid, Spain

ARTICLE INFO

Keywords:
Mars
Climate
Surface
Meteorology

ABSTRACT

Diurnal ground surface temperatures (T_g) and the five major terms of the surface energy budget (SEB) are displayed from hourly Mars Science Laboratory observations and from column model simulations in four contrasting cases along the Curiosity traverse. T_g and the SEB terms are otherwise well simulated on regolith near the landing spot and on rocky Pahrump Hills, but the residual in observation-based SEB (~downwelling longwave radiation) shows unexplained peaks in the morning and evening and simultaneously model-T_g is too cold. Enhanced or diurnally variable crater dust does not help but diurnally variable soil thermal inertia (suggested by Fourier analysis of observed T_g) reduces both defects at both sites. Sand on the steep Namib dune is instead homogeneous, defects here being reduced by taking into account slope effects. Regolith at the 2018 dust storm site appears inhomogeneous, with the SEB terms and T_g relatively well simulated even in this case of extremely heavy dust load.

1. Introduction

The Mars Science Laboratory (MSL) mission's rover, Curiosity, landed onto the equatorial Gale crater of Mars (4.6°S, 137°E) in August 2012. It carried the Rover Environmental Monitoring Station (REMS, Gómez-Elvira et al., 2012), which has since been measuring meteorological conditions every Mars hour. From these and other MSL observations it is now possible to estimate the diurnal and annual surface energy budgets along the Curiosity track, and compare them with predictions from numerical models for the martian atmosphere and ground. The energy budget of the surface is a strong driver for these models. As models are essential tools in interpreting observations and understanding the behavior of the martian atmosphere, such comparisons increase our knowledge and may also help to validate and perhaps improve these models.

Conservation of energy at the ground surface of Mars requires that at any time

$$G = SWD–SWU + LWD–LWU–TF–LF \quad (1)$$

where G is the heat flux into the ground, SWD the downwelling shortwave (solar) radiation transmitted through the atmosphere, SWU the upwelling solar radiation reflected by the ground, LWD the downwelling longwave (thermal infrared) radiation emitted by the overlaying atmosphere, LWU the upwelling longwave radiation emitted by the ground surface, TF the sensible heat flux associated with turbulent motions and LF the latent heat flux associated with moisture exchanges at the surface. TF is normally quite small and LF is insignificantly small at the low latitude of Gale. Eq. (1) is known as the surface energy balance (or budget), SEB.

There was no suitable instrumentation for LWD in Curiosity, but the other major SEB terms of (1), namely G, LWU, SWD, SWU and TF can be estimated using Mastcam 880 nm opacity (~τ_{vis}) and the REMS observations of UV radiation and ground and air temperatures (T_g, T_a), with some modeling. Martinez et al. (2021) described the methods and made a careful study of these SEB terms along the Curiosity track, using hourly data from the first 2500 MSL solar days (sols). This covers nearly four martian 669-sol years. The non-observed LWD was deduced as the residual in (1), discarding the tiny LF:

* Corresponding author at: INAR/Physics, Faculty of Science, University of Helsinki, 00014, Finland.
E-mail address: hannu.savijarvi@helsinki.fi (H.I. Savijärvi).

https://doi.org/10.1016/j.icarus.2022.114900
Received 1 October 2021; Received in revised form 13 January 2022; Accepted 13 January 2022
Available online 21 January 2022
0019-1035/© 2022 The Authors. Published by Elsevier Inc. This is an open access article under the CC BY license (http://creativecommons.org/licenses/by/4.0/).

$$LWD = G–SWD + LWU + SWU + TF \quad (2)$$

Values of the residual-LWD are hence sensitive to any inaccuracies in the right-hand-side terms.

The observation-based estimates for the six terms of (2) were mostly what could be expected on the basis of model simulations. A surprise was, however, that the residual-LWD (2) displayed systematic unexpected peaks during midmorning and late afternoon, whereas atmospheric models and model-based data assimilations (e.g. the Mars Climate Database) predict no such peaks. These LWD peaks were modest during the less dusty cool seasons at Gale, and stronger during the warm dusty seasons, being typically 10–30 W/m^2 (~30%) above the respective model-LWD values. A possibly related fact is that models, when validated by observed T_g along the Curiosity track, have tended to show cool T_g-biases during midmorning and late afternoon (e.g. Hamilton et al., 2014; Vasavada et al., 2017; Steele et al., 2017; Martinez et al., 2021).

Our goal is here to explain the model biases and to understand whether the peaks in the residual-based LWD are real, or result from inaccuracies in the other terms of the observation-based surface energy budget. We display the SEB terms and T_g from observations in four environmentally very different key cases along the Curiosity track, and make column model experiments. The first two cases, on regolith and on bedrock-with-fines ground, are from warm-season sites, in which the cool T_g-biases had been particularly persistent and large in the previous experiments of Hamilton et al. (2014) and Vasavada et al. (2017). The third case considers a sand dune site within the low-dust cool season, and the fourth case is on regolith during the peak of the 2018 dust storm.

The simulations are made with the University of Helsinki/Finnish Meteorological Institute single-column model (hereafter SCM, briefly described in Section 2). The T_g –predictions of SCM are compared to observed T_g from the REMS Ground Temperature Sensor device (GTS), and the model's SEB terms are compared to the respective observation-based values (providing here a novel opportunity to validate model-SWD against direct in-situ surface observations and model-LWD against the indirect residual-LWD). Our experiments concentrate on two hypotheses: 1) dust might be diurnally variable and enhanced within the crater (Section 4), and 2) ground might be inhomogeneous so that its thermal inertia is not diurnally constant (Section 5). The four cases are discussed in Sections 3–5, 6, 7 and 8, respectively. Conclusions are given in Section 9.

2. Model, methods, hypotheses and experiment design

The SCM is a hydrostatic air-soil column model without advections, having 29 grid points up to 40 km altitude in the air, and eight grid points in the soil down to 35 cm depth. It is forced by a constant geostrophic wind (here set to 10 m/s) and ground temperature T_g, which is driven by the model's surface energy budget. Parameterizations include a Monin-Obukhov surface layer and mixing-length Ekman layer turbulence, solar and thermal radiation, thermal diffusion in the ground, and moist physics. Solar radiation is via a fast broadband modified two-stream SW scheme (compared to results from spectrum-resolving multiple-stream radiation models (SRM) it has shown good accuracy, Savijärvi et al., 2005; Chen-Chen et al., 2021). The fast LW emissivity scheme takes into account CO_2, H_2O and dust (the dust-τ_{LW} /τ_{vis} -ratio optimized by comparison to results from the Crisp SRM). SCM has previously simulated the diurnal surface and boundary layer air temperatures quite well compared to MER mini-TES observations (Savijärvi, 2012a, 2012b).

The slope effects on SWD are here as by Mahrer and Pielke (1977). Slope angles and azimuths for the GTS field-of-view area (FOV) are from Vasavada et al. (2017), and for the UV sensor (UVS, on the rover deck) from the rover's current yaw, pitch and roll. The model's rover-tilted SWD is then compared to the UVS-based observed SWD, whereas the GTS FOV -tilted SWD is used in the simulations and the resulting T_g is compared to the GTS FOV observations.

The model is initialized with REMS-observed mean surface pressures (Harri et al., 2014) together with realistic vertical profiles for temperature, dust and moisture. It is then run with a 10 s time step to model sol 3, whereby it has spun up to a repeating diurnal cycle of winds, temperatures and moistures. Moisture is not considered here, as LF in insignificantly small in (1) but the modeled moisture cycles (with soil adsorption and desorption, which are sensitive to T_g) are shown and compared to in-situ moisture observations from MSL and Phoenix in Savijarvi et al. (2016, 2019, 2020); Savijarvi and Harri (2021).

The input values for dust (τ_{vis}, τ in short) and soil thermal inertia (I) are here our main suspects for the LWD peaks and T_g-biases. Diurnally constant values for τ and I are typically used in model simulations. Dust will be discussed in Section 4. Thermal inertia does depend on soil temperature in Mars but the diurnal effect on simulated T_g is small (Piqueux and Christensen, 2011) and can be excluded. Vasavada et al. (2017) experimented with layered I, i.e. vertically inhomogeneous soil. This removed the afternoon cold biases of T_g to a good extent, but not the morning biases. Putzig and Mellon (2007) modeled horizontally inhomogeneous (mixed) soil for remote sensing purposes. They found large diurnal effects on the resulting apparent I, due to low-I fractions of soil (e.g. dust and sand) typically cooling strongly at night, then warming rapidly in sunshine, whereas the high-I fractions (e.g. exposed bedrock) warmed and cooled more slowly. Horizontal mixtures of low-I materials (fines) and high-I bare rock are quite common in the GTS FOV images shown in Hamilton et al. (2014) and Vasavada et al. (2017).

We estimate here G from GTS observations by Fourier analyzing the diurnal cycle of the hourly means of T_g in each case. The resulting non-aliased Fourier series for T_g(h), h = 0,.., 23:

$$T_g(h) = T_m + \sum_{n=1}^{10}(A_n sin(x) + B_n cos(x).)$$

where T_m is the diurnal average and $x = n \cdot 2\pi h/24$, reproduces the observed means typically within ±0.3 K. Now, taking the linear soil thermal diffusion equation with constant thermal conductivity λ, volume heat capacity ρc and thermal inertia $I = (\lambda\rho c)^{1/2}$, each Fourier wave $T_{gn}(t)$ as the top boundary condition forces a well-known damped and delayed wave solution $T_n(z,t)$ into the soil. Setting these solutions to $G = -\lambda(\delta T/\delta z)_{z=0}$ leads via analytic differentiation and summing to:

$$G(h) = I \bullet \sum_{n=1}^{10}[C_n(A_n(\sin(x)+\cos(x)) + B_n(\cos(x)-\sin(x)))] = I \bullet S(h) \quad (3)$$

where $C_n = \sqrt{n}\cdot\pi/D$, D being the sol length, 88,775 s. For constant I the resulting G(h) is similar to a high-resolution numerical solution to the same problem (such as in Martinez et al., 2021). An advantage of (3) (on top of being an exact solution without finite differencing errors) is that approximate hourly values for apparent I can now be estimated by substituting (3) to Eq. (1), solving for I; I(h) = (SWD – SWU + LWD – LWU – TF)/S(h), and using the observed hourly means for SWD, SWU and LWU, and SCM values for LWD(h) and TF(h). The resulting hourly values of I are only approximate, as LWD and TF are from a model and the slopes of the UVS-based SWD and SWU may differ from the GTS-FOV based LWU and G. Nevertheless, such hourly estimates of apparent I may be informative and may be compared with the computational results of Putzig and Mellon (2007) for inhomogeneous soil.

We consider firstly MSL sols 30–37 near the Bradbury Landing site, where simulations with the KRC column model indicated systematic cool biases from 5 up to 17 K in T_g during midmorning in Hamilton et al. (2014) and Vasavada et al. (2017, V17 from now on). Although layering removed the respective afternoon biases to a good extent in V17, the large morning bias could not be explained by soil's vertical inhomogeneity or by values of slope, viewing angles or roughness consistent with imagery. Hence this case appears to be a good candidate for our SCM experiments.

3. Bradbury landing (BL)

Curiosity was stationary during sols 30–37 (L_s 170°-175°) about 30 m east of the Bradbury landing spot, midsol sun being near zenith at this time in Gale at 4.6°S. The full diurnal SEB data was available for five sols during the period. The site consists of loose-material regolith. We set here albedo A to 0.25 and thermal inertia I to 350 J m^{-2} K^{-1} $s^{-1/2}$ (SI units, units omitted hereafter) as indicated by the KRC simulation for homogeneous ground in V17. Tilt of the GTS scan area was here 3° down to northeast (57°), rover tilt being about the same. Dust opacity was moderate, around 0.65, and surface pressure about 7.5 mb.

Fig. 1 shows the observed hourly T_g from the five sols and from the SCM simulation for L_s 172° (thick line). This reference simulation uses the above constant input values and assumes well-mixed dust; thin line will be discussed in Section 5. The thick-line simulation matches the observed maxima and minima of T_g, but it displays cool biases in mid-morning and during the late afternoon, just like the KRC model simulations in Hamilton et al. (2014) and in V17.

Fig. 2 displays the observation-based hourly values of the two largest SEB terms LWU and SWD (symbols) together with model values (curves). Here LWU = $\varepsilon_g \sigma T_g^4$, using the GTS-observed and model's T_g; σ is the Stefan-Boltzmann constant and ε_g the ground emissivity of 0.97. LWU appears moderately well simulated, except during the cold biases. Observations of SWD are based on the REMS-UVS device measurements corrected for the spectral, angular and dust cover effects (Vicente-Retortillo et al., 2015, 2020), but not for rover tilt. The model's rover-tilted SWD-curve fits within the scatter of the five hourly observations in Fig. 2, except during midday, when it is an underestimate. Thin line shows model-SWD onto a horizontal surface (no slope). As the tilts of the rover and the GTS FOV are here nearly the same and quite small, the model's UVS- and GTS-slope curves of SWD fall together and are close to the horizontal SWD in Fig. 2, being slightly smaller in the afternoon when the ground is tilted away from the sun's westerly direction.

Fig. 3 displays the observation-based hourly 5-sol means of the three smaller SEB terms –SWU (= − A·SWD, minus sign for clarity), G (from (3)) and LWD (from (2)), with the respective model curves. SWU appears to be well modeled, G slightly less well. The black (filled) circles are the hourly 5-sol means of the residual-LWD from Eq. (2). They hover around the reference model's LWD (the thick curve), indicating however clear peaks at around 07–09 and 15–17 local mean solar time (LMST), and also a dip at 10–12 LMST. These peaks appear at the same time as the model's cool T_g-biases in Fig. 1. The open circles will be discussed in the end of Section 5.

4. Dust enhancement experiments at BL

The dust amount within the crater might be enhanced in the morning after the nocturnal convergence by the dust-transporting drainage winds

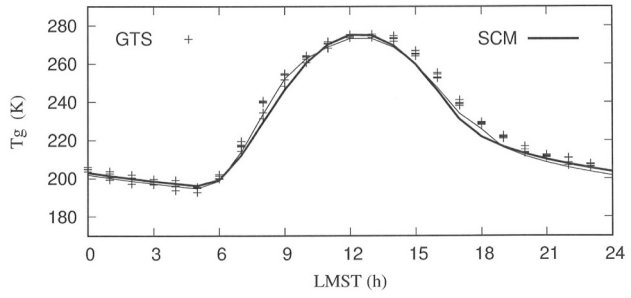

Fig. 1. Measured hourly (GTS) and modeled ground surface temperatures for MSL sols 30–37, L_s 170°-175°, Curiosity standing on regolith near Bradbury Landing. Thick curve is SCM simulation with albedo A = 0.25, soil thermal inertia I = 350 and dust opacity τ = 0.65. Thin curve is from a simulation with variable I (280–420) from Fig. 4.

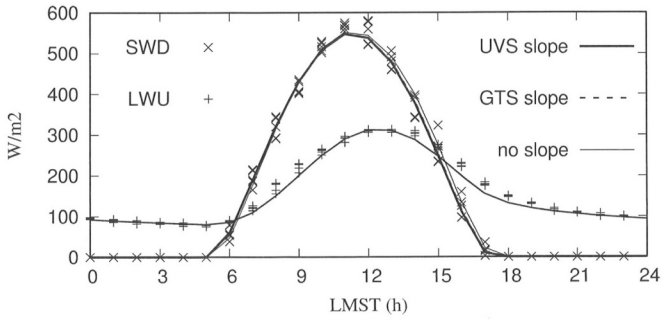

Fig. 2. Observation-based hourly downwelling shortwave radiation SWD from UVS and upwelling longwave radiation LWU at the surface from GTS during MSL sols 30–37. Model's SWD-curves are for a horizontal surface (no slope), for the tilted rover deck (UVS slope), and for the GTS scan area (GTS slope). The two slopes are here small (~3°) and about the same.

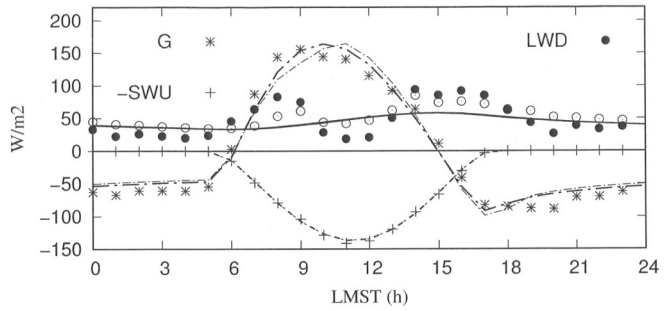

Fig. 3. Observation-based mean hourly values from sols 30–37 of heat flux into the ground G, upwelling solar radiation –SWU (minus sign for clarity) and the SEB residual (~ downwelling longwave radiation from the atmosphere LWD, black circles). Thick curves are from SCM simulation with I = 350, thin curves with variable I. Open circles are for residual-LWD, in the calculation of which the constant-I G-values (stars) are replaced by model-G from the variable-I experiment.

down the cold slopes of the crater walls and Mt. Sharp. On the other hand afternoon anabatic upslope flows might lead to compensating dust-concentrating downflow into the interior of the crater. Such local flows appear in the fine scale 3-D simulations of the Gale crater (Rafkin et al., 2016; Steele et al., 2017). They are similar to diurnal circulations that lead to heavy desert dust and industrial pollution during stagnant conditions in Earth valley cities (Savijärvi and Jin, 2001). Enhanced dust may induce extra solar heating, warmer air temperatures and hence increased LWD in the morning and evening, which might in turn heat the ground and remove the morning and afternoon biases.

We test firstly three time-constant dust profiles. In the first profile dust is assumed well mixed both horizontally and vertically: $\tau(z) = \tau_{vis} \cdot \exp.(-z/H)$, where H is the scale height of the atmosphere, 11 km. This profile was used in the above reference simulation. The other two profiles are the widely adopted Conrath dust profile, and a profile, where the low dust concentration is enhanced, being constant (because of strong daytime turbulence) up to 4 km height with constant extinction coefficient of 0.03 km^{-1}. This last profile is based on LIDAR observations and SCM experiments with a dust scheme at Phoenix (Savijärvi and Määttänen, 2010). It turned out, however, that all three simulations produce practically the same result. A realistic temporally constant low-dust enhancement therefore does not appear to produce LWD peaks, nor to remove the T_g-bias. Moreover, Rafkin et al. (2016) suggest that dust concentration might in fact be relatively low within the isolated Gale crater air, except perhaps around L_s 270°, when the crater is flushed by strong northeasterly large-scale winds.

Some UV and Mastcam/Navcam line-of-sight observations suggest

that dust opacity might be higher in the morning within the crater. A few time-dependent dust experiments ($\tau_{vis} = \tau_{vis}(t)$) were hence made, but the morning and evening enhancements of τ needed to produce the peaks in LWD were unrealistically high, 50–100%. Furthermore, even if LWD thereby increased, SWD decreased even more, because of strong SW extinction by the enhanced dust. As a result, the cold biases in T_g became worse. It thus appears that enhanced dust is not a good hypothesis for the peaks and biases.

5. Inhomogeneous ground at BL

In Putzig and Mellon's (2007) comprehensive numerical experiments for horizontally mixed soil (low I/high I during warm season at 30°S), the resulting apparent thermal inertia I was typically low from the evening to late morning, and higher in the afternoon. Around dawn and dusk the values of apparent I were less well defined and quite peaky.

Fig. 4 shows the hourly apparent I in the Bradbury Landing case as determined via the Fourier series method described in Section 2. Dashed line displays the constant value $I = 350$ used in the KRC and SCM simulations discussed above. That appears to be a good overall average, but at night I(h) is clearly below and from 11 LMST onward above it, being less well defined at around 06 LMST and 14–16 LMST (i.e., when G is small, Fig. 3). These features are consistent with Putzig and Mellon's results and suggest that the loose regolith at the Bradbury Landing site is a mixture of finer and coarser material.

We next ran SCM with a simple diurnally variable $I = 280$–420 (solid line in Fig. 4), which mimicks the basic features of the observation-based I(h). This simulation produces the thin-line T_g of Fig. 1. It clearly removes most of the morning cold bias. Hence this bias is presumably mainly due to the horizontal mixture of lower-I and higher-I materials within the GTS FOV scan area. The afternoon cold bias mostly remains. It was in turn cured by a vertical mixture in V17. Thus it seems that both horizontal and vertical mixtures are present even in a homogeneous-looking martian regolith, such as at Bradbury Landing. The amounts of cold T_g-biases in constant-I simulations might hence be used to chart the degree of inhomogeneity in the ground. Likewise, systematic differences in apparent I derived from orbital daytime and nighttime observations of T_g may indicate the same.

The thin dash-dot line in Fig. 3 displays model-G from the above variable-I experiment. It is close to the constant-I simulation (thick dash-dot line), differing from it mostly around midmorning and midday. Open circles in Fig. 3 are values for the residual-LWD, in the calculation of which via Eq. (2) these variable-I model values of G are used instead of the Fourier method G (Eq. (3)), which was based on constant I. The resulting open-circle LWD is smoother: the night values are now close to model-LWD; the morning and evening peaks are reduced and the midday dip is weaker as well. Hence the peaks and dips in the original residual-LWD are probably not real and at least partly due to inhomogeneity of regolith at the BL site, which then modifies the hourly values of G.

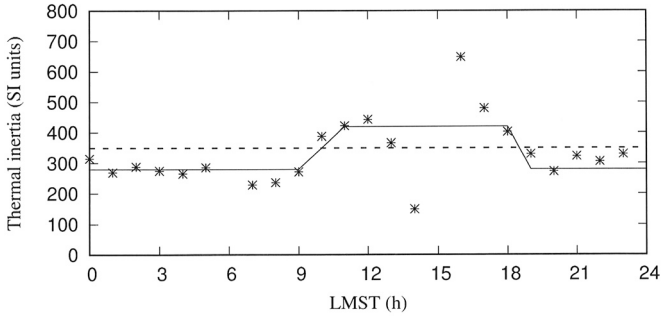

Fig. 4. Hourly soil thermal inertia I for sols 30–37 as derived via the Fourier series method of Section 2 (stars). Dashed line is the applied constant I, solid line is I used in the variable-I simulation. Note the tendency for low I at nighttime and midmorning, and high I in the afternoon.

6. Pahrump Hills

We consider next the well-documented rocky-region Pahrump Hills case of V17 within the warm and dusty perihelion-southern summer season. Here, during L_s 270°–290° on sols 865–895 Curiosity was stationary at a bedrock-with-fines region on the Murray formation (Pink Cliffs site) at Pahrump Hills. The ground was dominated by light-toned mudstone sloping gently upward to the south (Minitti et al., 2019). The KRC model simulation of V17 for homogeneous ground ($I = 340$, A = 0.26) clearly indicated cool T_g-biases in the morning and late afternoon. We adopt instead the THM-model constant values of V17 ($I = 400$, A = 0.25) for soil at this site with $L_s = 280°$, $\tau = 0.95$ and surface pressure p_s = 9.1 mb. The available nine sols of full diurnal cycle in the SEB data during this period provide the validating values.

Fig. 5 shows the observed values of diurnal T_g, sol-to-sol scatter being rather small. The relatively high values of surface albedo, thermal inertia and dustiness keep the diurnal amplitude of T_g in a moderate value despite the strong solar radiation of the season. The SCM simulation of T_g (thick line) displays a decent fit with observations, indicating however again cool biases during midmorning and in the late afternoon, like the homogeneous-ground KRC simulation of V17. The model's ground surface also appears to cool off slightly too slowly during the night, as if the value for thermal inertia (400) was too high.

Fig. 6 displays the observation-based hourly values of LWU and SWD from the nine sols (symbols) and from the SCM simulation (lines). LWU is again moderately well simulated, except during the cold biases of T_g. The top thin line shows the model's SWD onto a horizontal surface. The rover with the UVS sensor on it is here tilted about 8° down to northeast. The model's rover-SWD (thick line) appears to fit quite well within the SWD-observations. Model-SWD falling onto the GTS field of view (dashed line), which drives the T_g-simulation, is here slightly higher, due to the smaller FOV-plane tilt of 5.3° to 353°. Fig. 6 thereby demonstrates the effects of the two slopes on the downwelling solar radiation, and shows that the model's SW scheme is coping well in the current conditions of moderate dust ($\tau \sim 1$) and strong solar radiation.

Fig. 7 displays the hourly 9-sol means of –SWU, G and LWD from this period. SWU appears well modeled. Stars indicate G as estimated from observed T_g with the Fourier method (Eq. (3)), using the constant I of 400. Compared to these model-G is too high during the late evening and night, too low in midmorning but about right in the late afternoon. Black circles are the 9-sol hourly means of the observation-based residual-LWD. They hover around the model-LWD (thick line), being a lot smaller during the evening and night but once again displaying strong peaks in midmorning and late afternoon.

Fig. 8 shows the hourly I obtained via the Fourier method from the Pahrump Hills data. The values are low (around 300) during the night and morning, but increase to about 400 for the afternoon. This basic

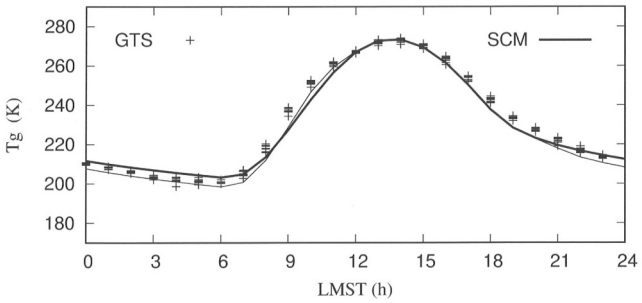

Fig. 5. As Fig. 1 but for the warm-season mudstone-with-fines Pahrump Hills site, MSL sols 865–895, L_s 270°-290°. A = 0.25, $\tau = 0.95$. Thick curve: $I = 400$, thin curve: I = variable 300–400.

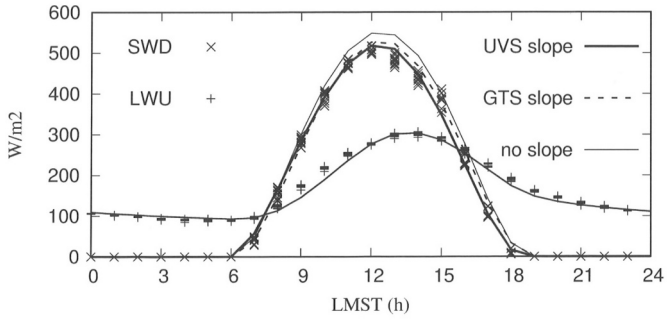

Fig. 6. As Fig. 2 but for the Pahrump Hills case. UVS slope is here 8° down to 45°, GTS scan area slope 5.3° down to 353°.

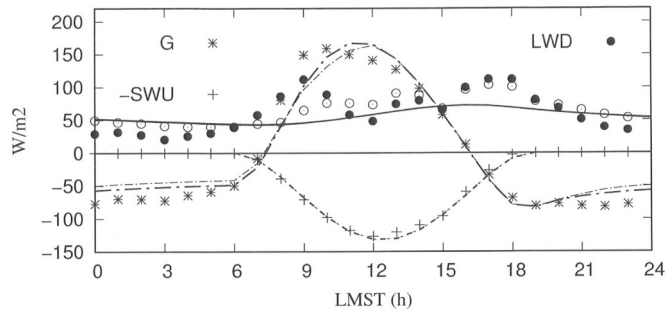

Fig. 7. As Fig. 3 but for the Pahrump Hills case.

diurnal variation (solid line) was then introduced to the SCM. The resulting T_g-simulation, the thin line in Fig. 5, appears to be closer to the observations, although the still too slow T_g-increase soon after the sunrise suggests that I should perhaps be made even lower at 08–09 LMST, as Fig. 8 suggests. A very low apparent I soon after sunrise was also typical in Putzig and Mellon's experiments.

When G from the variable-I simulation (thin dash-dot line in Fig. 7) replaces constant-I G in the residual estimation of LWD, the resulting values of LWD, open circles in Fig. 7, are a lot higher at night and the morning peak disappears. The afternoon LWD-peak remains, however, suggesting again that this peak and the remaining afternoon T_g-bias may be associated with vertical rather than horizontal inhomogeneity in the soil.

Hence both regolith around the Bradbury Landing and the bedrock-with-fines ground at Pahrump Hills appear to exhibit inhomogeneity. Inclusion of this in the form of diurnally variable schematic apparent thermal inertia improves simulations of T_g and reduces peaks in the residual-LWD.

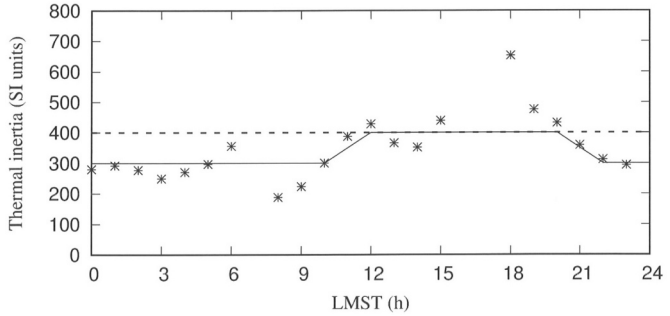

Fig. 8. As Fig. 4 but for the Pahrump Hills case.

7. Namib dune

Here a case of cool season, low dustiness and low thermal inertia on slant ground is demonstrated. Curiosity was standing stationary next to an active sand dune on sols 1222–1242 during the cool aphelion-southern winter season (L_s 96°-102°). The GTS device was viewing the steep west-facing slope (tilt ~10°) of the dark-sand Namib dune, with $I = 180$ and $A = 0.11$ from V17 adopted for the SCM simulation at L_s 100° ($\tau = 0.45$, $p_s = 8.3$ mb). The validating observational material consists here of the ten available sols of full diurnal cycles for the SEB terms. The rover was parked on flatter ground with downtilt of about 4° toward 240°.

Fig. 9 displays the ten hourly GTS-T_g observations and the simulated values. The combination of low solar radiation, low thermal inertia and low albedo of the dune, and low dustiness typical of the season leads here to cold nighttime and quite warm midday values of the dune-T_g. The simulation with constant I is here fairly accurate, suggesting that the sand on the active dune is rather homogeneous. One may note, however, that model-T_g displays weak cool bias at 07–08 LMST and warm bias at 10–12 LMST, as also did the homogeneous-soil KRC model simulation of V17.

The observation-based values of UVS SWD and the GTS FOV-plane LWU are fairly well simulated according to Fig. 10. Note that the west-facing GTS-sloped dune-SWD (dashed line) is here about 40 W/m^2 lower than the rover-SWD in the morning (sun being in the eastern sky), but then higher in the afternoon. Fig. 11 displays the hourly means of G, –SWU and LWD from observations (symbols) and the respective model values (curves). The observation-based residual-LWD (black circles) displays here only a very weak morning peak, but low (even unphysical negative) values during midmorning. The main reason is that it was obtained by applying the observed UVS-based SWD in Eq. (2), whereas SWD actually falling onto the west-facing GTS FOV-plane is as much as 40 W/m^2 lower in midmorning (Fig. 10). Replacing the UVS-SWD values by model's GTS-SWD in the calculation of the residual-LWD leads here to the open circles of Fig. 11. These values are nonnegative and closely follow the model's LWD, displaying however still a small dip at 10–12 LMST.

Fig. 12 presents the hourly thermal inertia values derived using the Fourier method for the Namib data (stars). The dune sand appears to be quite homogeneous, $I = 180$ being a good overall value. The values of I (h) are, however, somewhat higher before noon. Triangles represent here an otherwise similar I-calculation, but the observed rover-SWD is replaced by model's GTS SWD (dashed line in Fig. 10), which perhaps better represents the solar radiation falling onto the slant west-facing GTS FOV area. This does reduce the daytime scatter in I(h), hence making the dune look even more homogeneous. There remains, however, a tendency for low I at 07–08 LMST, and high I at 10–12 LMST. If put into the simulation, such I would probably reduce the model's small

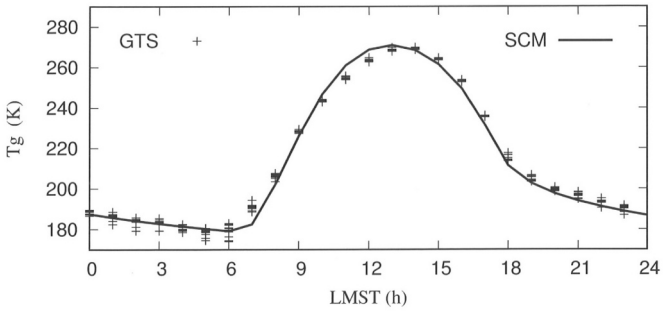

Fig. 9. As Fig. 1 but for a cool season dark sand dune site (Namib), sols 1222–1242, L_s 96°-102°. $I = 180$, $A = 0.11$, $\tau = 0.45$. Note the model's cool bias at 07–08 LMST and warm bias at 10–12 LMST. (For interpretation of the references to colour in this figure legend, the reader is referred to the web version of this article.)

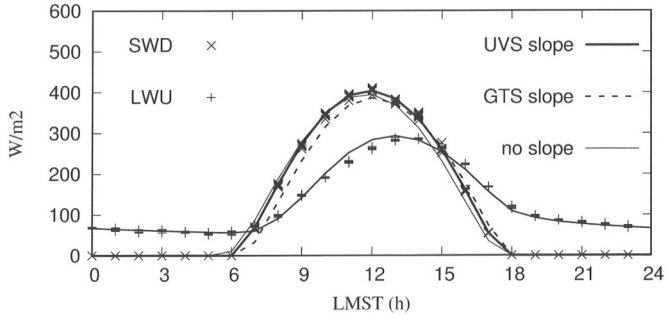

Fig. 10. As Fig. 2 but for the Namib dune case. GTS was scanning the west-facing ~10° slope of the dune whereas the rover with the UV sensor on its deck was standing on flatter ground.

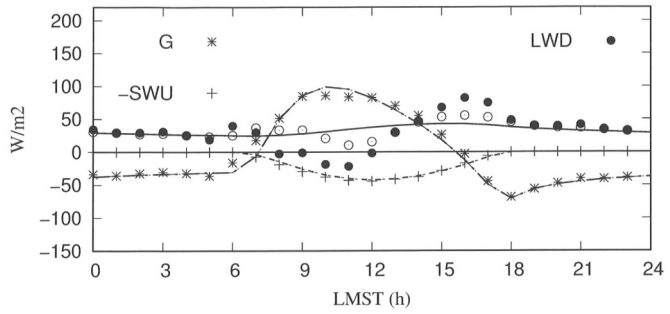

Fig. 11. As Fig. 3 but for the Namib dune case. Open circles represent here residual-LWD, in the calculation of which the observed rover-SWD is replaced by model-SWD onto the GTS slope.

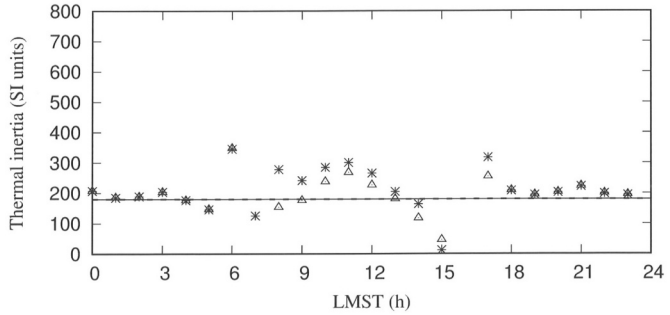

Fig. 12. As Fig. 4 but for the Namib dune case. Triangles are for I-estimate (Section 2), where the observed rover-SWD is replaced by model-SWD onto the GTS slope. Note the low thermal inertia at 07–08 LMST and high inertia at 10–12 LMST.

T_g-bias at these hours. Alternatively, if the well-sorted sand is assumed to be fully homogeneous, the scatter of I in Fig. 12 then provides an estimate for uncertainties in the data and methods.

In summary, T_g and SWD are here well simulated, the dune sand appears to be fairly homogeneous, and the slope effects on SWD are the dominating reason for the large daytime mismatch between the original observation-based residual-LWD and model-LWD. The small cool and warm morning biases in model-T_g are presumably related to the weak inhomogeneity of sand suggested by the Fourier method.

8. The 2018/MY34 planet-encircling dust event

Curiosity was moving on loose-material regolith at the foot of Vera Rubin ridge during the peak of the 2018/MY34 planet-encircling dust event (DE). The DE reached Gale on sol 2085 (L_s 195°), when τ_{vis} jumped from about 0.7 of the previous sols to 8.5–6.8 during the first five DE sols, with the T_g-amplitude suddenly decreasing from about 90 K to 30 K, then increasing slowly with decreasing τ (Guzewich et al., 2019). We present here the SEB values during the peak five sols 2085–2089, having $I = 200$, A = 0.17 (Martinez et al., 2021), $L_s = 197°$, $\tau_{vis} = 7.0$ and $p_s =$ 7.8 mb in the respective SCM simulation. The scale height of the dust is reduced from 11 km to 5.7 km in the model, whereby its temperatures at around the 30 km altitude better match those observed from orbit for the Gale latitude during the DE (Smith, 2019). As direct solar radiation is now nearly zero and diffuse radiation is highly isotropic in dense dust, slope effects on SWD are here irrelevant (slope angles are set to 0). This is fortunate as the rover was moving during the storm with the rover (UVS) and GTS tilts changing from sol to sol.

Fig. 13 shows the observed diurnal T_g during the GDE peak period, demonstrating the strongly reduced amplitude. The SCM ground temperatures (thick line) are close to those observed at night but the morning increase is slightly delayed and the afternoon values are too high. The reason is not in biased solar radiation as model-SWD is well within the scatter of observations in Fig. 14. Hence the model's fast broadband SW scheme appears to do a decent job even in this case of extreme dust load. The lowest observed values for SWD are from sol 2085 ($\tau = 8.5$) and the highest from sol 2089 ($\tau = 6.8$).

Fig. 15 displays the hourly means of G, -SWU and LWD from observations and from SCM. Observation-based values of G and SWU are fairly low and appear to be well simulated, although model-G is an overestimate in the early afternoon. In contrast, both the data-based residual-LWD and model-LWD are here quite high. The model values for T_g and LWD are surprisingly close to the observation-based values during the night (suggesting that the model's fast broadband LW scheme is also up to the task). Both of them are instead too high in the afternoon.

Fig. 16 presents the hourly apparent thermal inertia I as derived from observed T_g via the Fourier series method (Section 2). The values are low (below the average I = 200) during the night and very low soon after sunrise, then increase rapidly and are quite high in the afternoon. These high values might however be dubious, as the use of the too high model-LWD may feed back to them in the Fourier method. The high model-LWD of the afternoon might be due to too high boundary-layer air temperatures. This may force high T_g–values and these in turn the too high air temperatures. Unfortunately there are no mini-TES –like temperature soundings here to check this hypothesis.

The simulation with the variable I of Fig. 16 (solid line) produces an improvement to T_g (thin line in Fig. 13). Use of G from this simulation also reduces the gap between the resulting residual-LWD (open circles in Fig. 15) and the respective model-LWD (thin line in Fig. 15), but the gap is still present in the afternoon.

In short: the regolith appears to be inhomogeneous at the dust storm site and the column model produces a decent simulation even in this case of extremely heavy dust load.

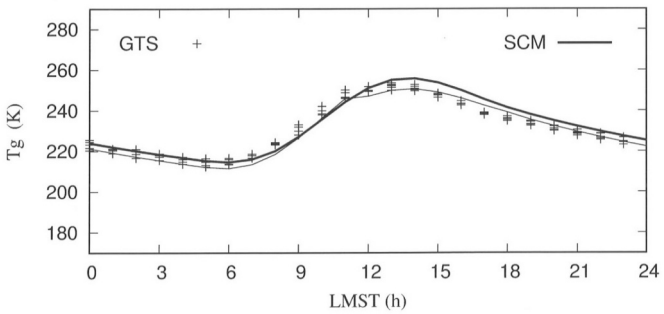

Fig. 13. As Fig. 1 but for the peak 5-sol period of the MY34/2018 global dust storm. $L_s = 197°$, A = 0.17, $\tau = 7.0$ in the SCM with $I = 200$ (thick line), I = variable (150–300, thin line).

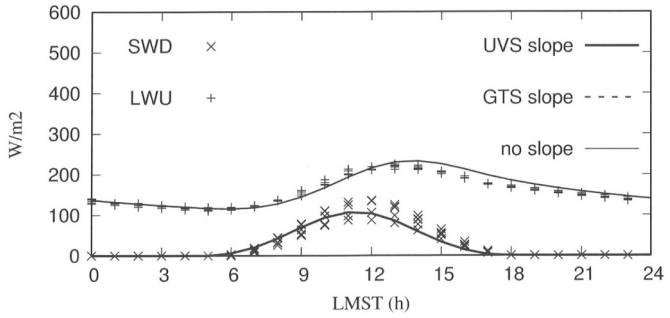

Fig. 14. As Fig. 1 but for the peak 5-sol period of the 2018 global dust storm. Observed τ is 8.5–6.8, with the lowest daily values of SWD for τ = 8.5 (sol 2085) and highest for τ = 6.8 (sol 2089).

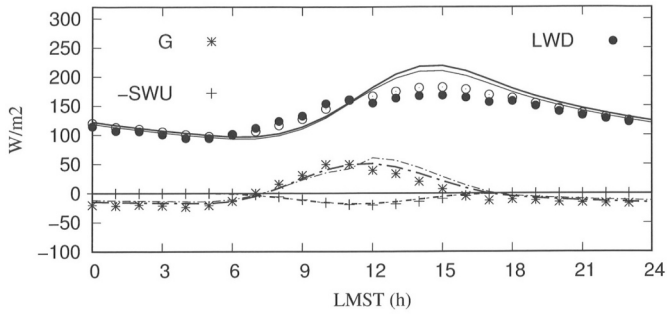

Fig. 15. As Fig. 3 but for the peak period of the 2018 global dust storm.

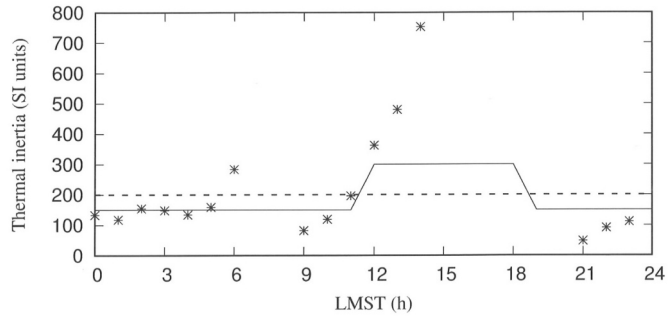

Fig. 16. As Fig. 4 but for the peak period of the 2018 global dust storm.

9. Summary and concluding remarks

Estimates for the surface energy budget from hourly Curiosity observations for 2500 sols in Martinez et al. (2021) raise the question for the reason of a systematic double-peak feature in the diurnal downwelling longwave radiation from the atmosphere, LWD. Atmosphere-soil models do not predict such morning and evening peaks but they do tend to underestimate the ground surface temperature T_g during the peak hours, when compared to observations of T_g from the Curiosity REMS-GTS device. Here we display the hourly T_g and the surface energy budget terms from MSL observations, and from single-column model simulations (using the UH/FMI SCM), in four quite different environmental conditions along the Curiosity track. We test two hypotheses for origin of the peaks in the residual-LWD of Martinez et al. (2021), and for the possible model biases.

Our model results with constant soil thermal inertia I are in general close to the observation-based values of T_g and SEB at the regolith-dominated Bradbury Landing region in $L_s \sim 170^o$, and at the bedrock-with-fines Pahrump Hills region in $L_s \sim 280^o$. However, like in previous KRC model simulations for these sites, they clearly display cool T_g –biases in the morning and evening. During the same hours there are strong peak values in the observation-based residual-LWD, which are not present in model-LWD.

The first hypothesis, enhanced time-variable dust within the crater, did not help according to model experiments. Enhanced dust did increase thermal radiation from the atmosphere, leading to peaks in the model-LWD, but it decreased the current model-SWD even more, so that the cool midmorning and afternoon biases in model-T_g became worse.

Our second hypothesis was that soil might be inhomogeneous, so that its apparent thermal inertia I might exhibit diurnal variation. The analytic Fourier time series method (Section 2) of deriving the ground heat flux G for constant I from observations of T_g also provided a possibility to find approximate hourly values for apparent I. These exhibited diurnal variations, which are consistent with the computational results of Putzig and Mellon (2007) for apparent I in horizontally mixed soil. When the basic feature, low I at night until late morning and high I in the early afternoon, was introduced into the simulations, the T_g-biases became a lot smaller, especially in the morning. Use of model-G from this variable-I experiment instead of the observation-based constant-I G also reduced the peaks in the resulting residual-LWD. It thus looks plausible that using diurnally constant thermal inertia for in reality inhomogeneous ground leads to: 1) biases of T_g in numerical models, and 2) biases of G when G is estimated from observed T_g. This in turn leads to the unreal peaks in the residual-LWD.

Our third case was on Namib sand dune, where the rover was standing next to the dark dune with GTS viewing its steep slope. Here the simulation of T_g with constant I proved out to be quite good, when sloping of the dune was duly taken into account. Sand appeared to be fairly homogeneous in the GTS scan area, displaying nearly constant low apparent I by the Fourier method. The observation-based residual-LWD showed here only very weak morning peak (consistent with homogeneous soil) but displayed an afternoon peak and low, even negative values around midday. These defects were much smaller when using in the residual-LWD calculation the model-SWD onto the slant dune, instead of the observed solar flux onto the rover deck on flatter ground.

The fourth case concerned the peak five sols of the 2018/MY34 dust storm, when dust opacity was 8.5–6.8 at Gale. Regolith of the site appeared quite inhomogeneous but peaks in the residual-LWD were nevertheless absent, presumably obscured by the very low values of G and solar radiation, and the massive values of thermal radiation from the dusty atmosphere.

In short, diurnally variable dust opacity did not reduce the simultaneous biases of residual-LWD and model-T_g, whereas taking into account heterogeneous regolith clearly improved matters at Bradbury Landing and Pahrump Hills. The slope effects on SWD may also be quite important in the local surface energy budget and T_g, as demonstrated by the uneven Namib dune ground. The model's fast radiation schemes appeared to do a good job, by these first-ever in-situ surface validations for Mars, the daytime LWD biases during the dust storm leaving scope for future work.

Acknowledgements

HS and AMH acknowledge the Academy of Finland grant 310529. AVR is supported by AEI project MDM-2017-0737 Unidad de Excelencia "María de Maeztu" - Centro de Astrobiología (INTA-CSIC). G. M. Martínez acknowledges support from Jet Propulsion Laboratory grant 1449038 and LPI/USRA Subaward No. Subk00011877. This is LPI Contribution no. 2658.

References

Chen-Chen, H., Perez-Hoyos, S., Sanchez-Lavega, A., 2021. Assessing multi-stream radiative transfer schemes for the calculation of aerosol radiative forcing in the Martian atmosphere. J. Geophys. Res. Planets 126, e2021JE006889. https://doi.org/10.1029/2021JE007889.

Gómez-Elvira, G.J., et al., 2012. REMS: the environmental sensor suite for the mars science laboratory rover. Space Sci. Rev. 170, 583–640. https://doi.org/10.1007/s11214-012-9921-1.

Guzewich, S.D., et al., 2019. Mars science laboratory observations of the 2018/Mars year 34 global dust storm. Geophys. Res. Lett. 46, 71–79. https://doi.org/10.1029/2018GL080839.

Hamilton, V.E., et al., 2014. Observations and preliminary science results from the first 100 sols of MSL rover environmental monitoring station ground temperature sensor measurements at Gale crater. J. Geophys. Res. Planets 119, 745–770. https://doi.org/10.1002/2013JE004520.

Harri, A.M., et al., 2014. Pressure observations by the curiosity rover: initial results. J. Geophys. Res. Planets 119, 82–92. https://doi.org/10.1002/2013JE004423.

Mahrer, Y., Pielke, R., 1977. The effects of topography on sea and land breezes in a two-dimensional numerical model. Mon.Wea.Rev. 105, 1151–1162.

Martinez, G.M., et al., 2021. The surface energy budget at Gale crater during the first 2500 sols of the Mars science laboratory mission. J. Geophys. Res. Planets 126. https://doi.org/10.1029/2020JE006804.

Minitti, M.E., et al., 2019. Distribution of primary and secondary features in the Pahrump Hills outcrop (Gale crater, Mars) as seen in a Mars descent imager (MARDI) "sidewalk" mosaic. Icarus 328, 194–209.

Piqueux, S., Christensen, P.R., 2011. Temperature-dependent thermal inertia of homogeneous Martian regolith. J. Geophys. Res. Planets 116. https://doi.org/10.1029/2011JE003805.

Putzig, N.E., Mellon, M.T., 2007. Thermal behavior of horizontally mixed surfaces on Mars. Icarus 191, 52–67.

Rafkin, S., et al., 2016. The meteorology of gale crater as determined from rover environmental monitoring station observations and numerical modeling. Part II: Interpretation. Icarus 280, 114–138. https://doi.org/10.1016/j.icarus.2016.01.03.

Savijärvi, H., 2012a. Mechanisms of the diurnal cycle in the atmospheric boundary layer of Mars. Quart. J. Roy. Meteor. Soc. 138, 552–560. https://doi.org/10.1002/qj.930.

Savijärvi, H., 2012b. The convective boundary layer on Mars: some 1-D simulation results. Icarus 221, 617–623.

Savijärvi, H., Harri, A.M., 2021. Water vapor adsorption in Mars. Icarus 327, 114270. https://doi.org/10.1016/j.icarus.2020.114270.

Savijärvi, H., Jin, L.Y., 2001. Local winds in a valley city. Boundary-Layer Meteor. 100, 301–319.

Savijärvi, H., Määttänen, A., 2010. Boundary-layer simulations for the Mars Phoenix lander site. Quart. J. Roy. Meteor. Soc. 136, 1497–1505. https://doi.org/10.1002/qj.650.

Savijärvi, H., Crisp, D., Harri, A.M., 2005. Effects of CO_2 and dust on present-day solar radiation and climate in Mars. Quart. J. Roy. Meteor. Soc. 131, 2907–2922.

Savijärvi, H., Harri, A.M., Kemppinen, O., 2016. The diurnal water cycle at curiosity: role of exchange with the regolith. Icarus 265, 63–69. https://doi.org/10.1016/j.icarus.2015.10.008.

Savijärvi, H., McConnochie, T., Harri, A.M., Paton, M., 2019. Annual and diurnal water vapor cycles at curiosity from observations and column modeling. Icarus 319, 485–490. https://doi.org/10.1016/j.icarus.2018.10.008.

Savijärvi, H., Martinez, G., Fischer, E., Renno, N., Tamppari, L., Zent, A., Harri, A.M., 2020. Humidity observations and column simulations for a warm period at the Mars Phoenix lander site: constraining the adsorptive properties of regolith. Icarus 343, 113688. https://doi.org/10.1016/j.icarus.2020.113688.

Smith, M.D., 2019. THEMIS observations of the 2018 Mars global dust storm. J. Geophys. Res. Planets 124. https://doi.org/10.1029/2019JE006107.

Steele, L.J., Balme, M.R., Lewis, S.R., Spiga, A., 2017. The water cycle and regolith-atmosphere interaction at Gale crater, Mars. Icarus 280, 56–79.

Vasavada, A.R., Piqueux, S., Lewis, K.W., Lemmon, M.T., Smith, M.D., 2017. Thermophysical properties along Curiosity's traverse in Gale crater, Mars, derived from the REMS ground temperature sensor. Icarus 284, 372–386.

Vicente-Retortillo, Á., Valero, F., Vázquez, L., Martínez, G.M., 2015. A model to calculate solar radiation fluxes on the Martian surface. J. Space Weather Space Clim. 5, A33.

Vicente-Retortillo, A., Martínez, G.M., Rennó, N.O., Lemmon, M.T., de la Torre-Juárez, M., Gómez-Elvira, J., 2020. In situ UV measurements by MSL/REMS: dust deposition and angular response corrections. Space Sci. Rev. 216 (5), 1–19.